NASA TECHNICAL NOTE

NASA TN D-2282

STATIC STABILITY CHARACTERISTICS OF BLUNT LOW-FINENESS-RATIO BODIES OF REVOLUTION AT A MACH NUMBER OF 24.5 IN HELIUM

by Robert D. Witcofski and William C. Woods

Langley Research Center

Langley Station, Hampton, Va.

NATIONAL AERONAUTICS AND SPACE ADMINISTRATION • WASHINGTON, D. C. • MAY 1964

STATIC STABILITY CHARACTERISTICS OF BLUNT LOW-FINENESS-RATIO BODIES OF REVOLUTION AT A MACH NUMBER OF 24.5 IN HELIUM

By Robert D. Witcofski and William C. Woods

Langley Research Center
Langley Station, Hampton, Va.

NATIONAL AERONAUTICS AND SPACE ADMINISTRATION

For sale by the Office of Technical Services, Department of Commerce,
Washington, D.C. 20230 -- Price $1.25

STATIC STABILITY CHARACTERISTICS OF BLUNT LOW-FINENESS-RATIO BODIES OF REVOLUTION AT A MACH NUMBER OF 24.5 IN HELIUM

By Robert D. Witcofski and William C. Woods
Langley Research Center

SUMMARY

A systematic investigation has been conducted at a Mach number of 24.5 in helium to determine the static aerodynamic stability characteristics of several series of blunt bodies of revolution, having fineness ratios of 0.50 and 1.00. The angle-of-attack range covered in the investigation was from 0° to 20°. The Reynolds number, based on maximum body diameter, varied from 0.26×10^{6} to 0.45×10^{6}, depending on model size. All bodies used in the investigation were stable in pitch about a point one-third the body length from the nose. The effects of nose corner rounding of flat-faced and spherical-faced cylinders and the effects of changing the exponent of bodies generated by the power-law equation have been determined. A sufficient number of shapes were tested within each of these classes to allow the determination of the aerodynamic characteristics of any shape, provided only that the shape lie within one of the three given classes. The static stability of blunted cones and cylinder-cone frustums was also determined for half-angles of 0°, 15°, and 30°. Comparison of data is made with results obtained from modified Newtonian theory. Theory generally underpredicted normal force and overpredicted axial force but agreement of theory and experiment improved as bluntness was decreased. A comparison of the present data with data obtained at a Mach number of 3.55 in air indicated a sizable difference in normal force and stability in pitch. This difference was attributed largely to induced pressure effects.

INTRODUCTION

When the designer selects a configuration for either a manned or unmanned entry into the atmosphere of the Earth or one of the other planets, the selection is complicated by a great many requirements. The state of the art of launch vehicles will be the most significant factor determining how much the configuration can weigh. Of importance, with reference to aerodynamic heating, are drag coefficient and ballistic coefficient, as was shown in reference 1. The first unmanned missions to planets other than the Earth will probably use a passive entry, that is, the entry trajectory will be determined by the basic

aerodynamic characteristics of the body. A knowledge of the various aerodynamic parameters involved in the calculation of the motion of an entry body must be available if the attitude and flight path of the vehicle are to be predicted with any accuracy.

The purpose of this paper is to supply information on the static stability characteristics, in the entry Mach number region, of a group of low-fineness-ratio bodies having a wide range of nose shapes and drags. The lifting capabilities of a configuration will largely determine the maneuverability and the breadth of the entry corridor (ref. 2). It has been shown in references 3 and 4 that, from the standpoint of dynamic stability, it is advantageous for entry bodies to develop a positive lift-curve slope, in that the positive lift-curve slope tends to offset the destabilizing effects of high drag coefficient. Entry into the atmosphere of planets other than the Earth will be further complicated by the, at present, incomplete knowledge of the density, gas composition, and temperature of the atmosphere surrounding these planets. (Ref. 5 suggests that the atmosphere of the planet Jupiter, for instance, may be as much as 97 percent helium.) Nose shapes and nose drags suitable for entry into these atmospheres may differ from those suitable for entry into the Earth's atmosphere, depending upon the type of mission undertaken. For this reason it would be advantageous to have performance information on vehicles covering a wide range of drag coefficients.

A systematic investigation of the static stability characteristics of several series of blunt low-fineness-ratio bodies of revolution has been conducted in the Langley 22-inch helium tunnel at a nominal free-stream Mach number of 24.5. Helium was used as a test medium because of the relative ease with which high Mach numbers can be obtained in this gas. The series consisted of an investigation of the effects of varying the corner radius of flat-faced (right-circular) cylinders, corner radius of spherical-faced cylinders, and the variation of the exponent n for power-law bodies ($n = 1, 2, 4, 6, 8$, and 10). These models were tested for fineness ratios of 0.5 and 1.0. Also investigated were the effects of varying the half-angle of blunted cones and the afterbody half-angle of cylinder-cone frustums. Fineness ratios ranged from 0.37 to 1.0 and 0.63 to 1.0 for the blunted cones and cylinder-cone frustums, respectively. The tests covered an angle-of-attack range of 0° to 20°, and Reynolds number, based on maximum body diameter, varied from 0.26×10^6 to 0.45×10^6, depending on model size.

A comparison of the data is made with calculations obtained from modified Newtonian theory. The static stability characteristics of this same series of bodies were determined previously at a Mach number of 3.55 in air (ref. 6) and a brief comparison of these characteristics with some of the data from the present test is made.

SYMBOLS

A	area of model base, sq in.
a	constant in equation of generating curve ($x = ar^n$) for exponential body shapes ("a" is determined in order to have bodies with $l/d = 0.5$ or 1.0)
C_A	axial-force coefficient, $F_A/q_\infty A$
$C_{A,\alpha=0}$	axial-force coefficient for angle of attack of 0°
C_D	drag coefficient, $C_A \cos \alpha + C_N \sin \alpha$
C_L	lift coefficient, $C_N \cos \alpha - C_A \sin \alpha$
C_{L_α}	lift-curve slope at $\alpha = 0^\circ$, per deg
C_m	pitching-moment coefficient about a point one-third of length rearward from face, on center line, $M_Y/q_\infty Ad$
C_{m_α}	slope of curve of pitching-moment coefficient with angle of attack at $\alpha = 0^\circ$, per deg
C_N	normal-force coefficient, $F_N/q_\infty A$
C_{N_α}	slope of curve of normal-force coefficient with angle of attack at $\alpha = 0^\circ$, per deg
d	maximum body diameter, in.
d'	diameter of basic body, in.
F_A	axial force, lb
F_N	normal force, lb
l	length of model, in.
l/d	fineness ratio
l/d'	basic fineness ratio
L/D	lift-drag ratio, C_L/C_D

M_Y	pitching moment about a point one-third of length of model rearward from face, on model center line, in-lb
M_∞	free-stream Mach number
n	exponent in equation of generating curve ($x = ar^n$)
q_∞	free-stream dynamic pressure, lb/sq in.
r	local radius of body, in.
r_1	radius of spherical face of spherical-faced cylinder, cylinder-cone frustum, and blunted cone, in.
r_2	radius of corner of nose of cylinder, cylinder-cone frustum, and blunted cone, in.
r_3, r_4	radii shown in sketch of figure 1(b)
S_s	area of model surface (including base), sq in.
V	volume of model, cu in.
x	distance along body longitudinal axis, measured from nose of body, in.
$\frac{x_{cp}}{l}$	location of center of pressure, determined by dC_m/dC_N at zero angle of attack, expressed in body lengths from nose
α	angle of attack, deg
θ	afterbody half-angle of blunted cones and cylinder-cone frustum, deg
$\frac{V^{2/3}}{C_D A}$	dimensionless modified ballistic coefficient (constant density assumed)
$\frac{V^{2/3}}{S_s}$	volume-area ratio (nondimensional)

APPARATUS AND TESTS

Models

The models tested were blunt low-fineness-ratio bodies of revolution, constructed of stainless steel. The series consisted of flat-faced (right-circular) cylinders with variations in corner radii, spherical-faced cylinders

with variations in corner radii, a group of exponential shapes, blunted cones with variations in half-angle, and cylinder-cone frustums with variations in afterbody half-angle. Bodies with fineness ratios of 0.5 and 1.0 were investigated for the studies concerned with variations in corner radii and exponential shapes.

The corner-radius study models consisted of putting nose corner radii of 0 (cylinder), 0.20d, 0.38d, and 0.50d (hemisphere-cylinder for $l/d = 1.00$, hemisphere for $l/d = 0.5$) on flat-faced cylinders and spherical-faced cylinders having $r_1 = d$. Sketches of these models are shown in figures 1(a) and 1(b). Figure 1(c) illustrates the exponential shapes. These models were formed by revolving the curve generated by the equation $x = ar^n$ about the X-axis. The values of n were 1 (cone), 2 (parabola), 4, 6, 8, and 10.

In the case of the blunted cones and the cylinder-cone frustums, fineness ratio is referred to in two forms: The form l/d' refers to fineness ratio determined from the length-diameter ratio of the basic body ($\theta = 0^\circ$) and the form l/d refers to the actual fineness ratio of the individual bodies. The blunted cones were formed by adding conical skirts tangent to the nose of a cylinder having a spherical face $\left(r_1/d = 1.00\right)$ and a rounded corner $\left(r_2/d = 0.20\right)$. Models with half-angles of 0°, 15°, and 30° and values of l/d' of 0.50 and 1.00 were tested. Sketches of the blunted cones, along with the corresponding values of l/d, are shown in figure 1(d).

The cylinder-cone frustums were formed by adding 15° and 30° half-angle skirts at $l/2$ of a spherical-faced cylinder having a nose radius $r_1/d = 1.00$ and a corner radius of $r_2/d = 0.20$. A fineness ratio of $l/d' = 1.0$ only was used for the cylinder-cone frustum. A sketch of these models along with the corresponding values of l/d are shown in figure 1(e).

For all models, the moment reference center selected was at a point one-third body length from the nose.

Facility and Instrumentation

The investigation was conducted in the Langley 22-inch helium tunnel at a Mach number of 24.5. A 5° half-angle conical nozzle was employed which produces a longitudinal test section Mach number gradient of about 0.08 per inch. The effect of this gradient, when the relative size of the test models (1.25-inch-diameter model in a 22-inch test section) is considered, is believed to be negligible. Also inherent in the conical nozzle is a flow divergence, which likewise is considered to be negligible. Further details concerning this facility may be obtained in reference 7. Stagnation pressure for the tests was 1,000 pounds per square inch gage. Stagnation temperature decreased about 20° F during each test because of the decreasing reservoir pressure, and an average stagnation temperature of 70° F was chosen as being representative. Reynolds number, based on maximum body diameter, varied from 0.26×10^6 to 0.45×10^6, depending on the individual model size.

The data were obtained by using a three-component strain-gage balance. The angles of attack ranged from 0° to 20° and were continuously changing during each test. Samples of data were taken at discrete angles of attack by utilizing the optical data acquisition systems described in reference 7.

Accuracy

The three-component strain-gage balance used to measure the forces and moments in this investigation had an accuracy of ±1.0 percent. Assuming an average model base diameter of 1.250 inches, the accuracy of the forces and moments measured by the balance and converted to coefficient form is as follows: For C_N, ±0.009; for C_A, ±0.018; and for C_m, ±0.007. When the transfer of moment reference center is made from the balance to the model center of gravity selected, an additional possible error in C_m is introduced due to the possible error in C_N. When this is taken into account, the probable accuracy of C_m is ±0.012. Figure 2 is a sketch of the model, balance, and sting assembly. It is difficult to estimate the accuracy in angle of attack when the present system as described in reference 7 is used, but it is believed that angle of attack is accurate to at least $\pm 0.2^\circ$. Base pressures were not measured and the data are not adjusted to free-stream conditions.

RESULTS AND DISCUSSION

The basic longitudinal characteristics of all the models tested are presented in figures 3 to 7. It is of interest to note that in these basic data plots, in general, the data are linear, or near linear, up to an angle of attack of 8° or 10° and, in some cases, this linearity extends over the entire angle-of-attack range covered in this investigation (up to 20°). Because of this linearity many of the stability parameters measured at $\alpha = 0^\circ$ will be applicable at an angle of attack of 10° or greater, and primary conclusions can be drawn from the summary plots, which are presented in figures 8 to 12.

Included in the summary plots are the effect of model geometry on C_{N_α}, C_{l_α}, C_{m_α}, $C_{A,\alpha=0}$, the location of center of pressure, the ballistic coefficient, and the ratio of internal volume to surface area. Location of center of pressure was determined by dC_m/dC_N at zero angle of attack and is expressed in body lengths from the nose. Ballistic coefficient is presented in the modified nondimensional form $\frac{V^{2/3}}{C_D A}$ in order to facilitate the practical application of this parameter. The nondimensional form of the volume-area ratio is presented as $\frac{V^{2/3}}{S_s}$, and is a rough measure of the ratio of the available internal packaging volume to the structural weight of a vehicle, large values of $\frac{V^{2/3}}{S_s}$

usually being desirable. It is of particular interest to note that in the case of the flat-faced cylinders, the spherical-faced cylinders, and the exponential shapes, a sufficient number of bodies were investigated within each class of shapes to permit the determination of the aerodynamic characteristics of any shape by merely fairing curves through the summary plots, the only provision being that the shape being considered lie within one of the above classes.

Modified Newtonian theory calculations are included in the plots and were obtained by the method described in reference 8 together with an additional modification to account for the contribution of axial force to pitching moment. In the summary plots, modified Newtonian calculations were obtained only for body shapes corresponding to those experimentally investigated and curves have been faired through the theoretical points to show trends.

Flat-Faced and Spherical-Faced Cylinders

The effects of variation of corner radius on the static stability characteristics of flat-faced and spherical-faced cylinders are presented in figures 8 and 9, respectively. Many of the aerodynamic trends have linear, or near linear, variation with r_2/d with the exception of the case of zero corner rounding. A comparison of figures 8 and 9 indicates that replacing the flat face on the cylinders with a nose radius of 1 base diameter had only small effects, the effects diminishing as corner radius was increased and the geometry of the two classes became more similar. An underprediction of the normal-force-curve slope by modified Newtonian theory, on the more blunt bodies, where the shock-wave standoff on the afterbody section is very large, is clearly illustrated in figures 8(a) and 9(a), where the addition of a cylindrical section of $d/2$ to the length of the fineness-ratio-0.5 bodies has a negligible effect on the theoretical value of C_{N_α}. However, increasing fineness ratio from 0.5 to 1.0 produced a positive shift in the experimental values of C_{N_α} that is approximately equal to the value of C_{N_α} obtained by the flat-faced cylinder of length $d/2$, as would be expected.

Exponential Shapes

It would appear (see fig. 5(b)) that maximum values of C_L and L/D may have been reached on the bodies having a fineness ratio of 0.5 for $n = 2$ and 4. In the summary plots of the exponential bodies (fig. 10), the results are plotted against $1/n$ and the flat-faced cylinder from the corner-radius study is taken as the case where $n = \infty$ and provides an end point of $1/n = 0$ for the data. Simple equations could be empirically derived for C_{N_α} and $C_{A,\alpha=0}$ for both fineness ratios and they are as follows:

For $l/d = 0.5$:

$$C_{N_\alpha} = 0.0208\left(\frac{1}{n}\right)^{0.272} \qquad (2 < n < 10) \qquad (1)$$

$$C_{A,\alpha=0} = 0.526(n)^{0.246} \qquad (4 < n < 10) \qquad (2)$$

For $l/d = 1.0$:

$$C_{N_\alpha} = 0.0255\left(\frac{1}{n}\right)^{0.272} \qquad (1 < n < 10) \qquad (3)$$

$$C_{A,\alpha=0} = 0.241(n)^{0.537} \qquad (2 < n < 10) \qquad (4)$$

Note, from equations (1) and (3) that for the fineness ratios of this investigation and for any value of n within the given limits, the value of C_{N_α} is a function of fineness ratio only. For each fineness ratio, the $n = 1$ (cone) bodies are seen to be the most stable in pitch; for the fineness ratio of 1.0, the cone bodies obtained the highest normal-force-curve and lift-curve slopes. Though these are favorable traits, a penalty is paid in that these cones have the lowest values of $\frac{V^{2/3}}{S_s}$ for this particular family. (See fig. 10(c).) Note also the low value of the modified ballistic coefficient obtained by the cones. The $n = 2$, $l/d = 1.0$ body exhibited relatively high lift, high stability in pitch, the lowest drag obtained $\left(C_{A,\alpha=0} = 0.35\right)$, the highest modified ballistic coefficient obtained $\left(\frac{V^{2/3}}{C_D A} = 1.95\right)$, and a reasonably high value of $\frac{V^{2/3}}{S_s}$. This body is close to the minimum drag body, $n = 3/2$, predicted by Cole in reference 10.

Data obtained for these same exponential shapes at a Mach number of 3.55 in air (ref. 6) are included in figures 10(a) and 10(b). Modified Newtonian theory implies that the forces exerted on a body, particularly in the region of large incidence with the flow, should depend only upon the value of maximum pressure coefficient selected. (Maximum pressure coefficients for the present tests and those at $M_\infty = 3.55$ were 1.76 and 1.88, respectively.) For low-fineness-ratio bodies, when the major portion of the body surface has large incidence with the flow, the data obtained at $M_\infty = 24.5$ in helium should not differ greatly from those obtained at $M_\infty = 3.55$ in air. This is seen, in figure 10(a), to be the case. As fineness ratio is increased the stability characteristics will be dictated to a large extent by the pressure distribution on the afterbody section or sections with low incidence to the flow. It was pointed out in reference 11 that for a typical blunt body (hemisphere-cylinder),

Mach number has a great effect on the nature of the induced flow field. The sizable difference in the data for the body with a fineness ratio of 1.0 at a Mach number of 24.5 in helium and 3.55 in air may be attributed to the differences in induced flow fields.

Half-Angle of Blunted Cones

In examining the results obtained on the blunted cones it should be pointed out that the coefficients are based on maximum base areas and diameters. Obviously the results obtained from using constant reference areas and lengths instead of the individual body base would be quite different. Note, in figure 11, that although the $\theta = 30^{\circ}$ bodies exhibited more lifting capabilities and were more stable in pitch, for each individual fineness ratio, the value of the modified ballistic coefficient, as well as the ratio of internal volume to surface area, was lower for these bodies. It is interesting to note that for the values of θ of this investigation, C_{l_α} had a near-linear variation with θ.

Half-Angle of Cylinder-Cone Frustum

A check run was made on the 15° cylinder-cone frustum and the data from the check run are presented in figure 7 as flagged symbols. Figure 12 indicates that increasing the half-angle of these cylinder-cone frustums from 0° to 30° produced increases in lift-curve slope, increases in stability in pitch, a decrease in $C_{A,\alpha=0}$, a rearward movement of center of pressure, and a decrease in the ratio of internal volume to surface area.

SUMMARY OF RESULTS

The static stability characteristics of several series of blunt low-fineness-ratio bodies of revolution have been determined at a Mach number of 24.5 in helium at angles of attack from 0° to 20°. Bodies with fineness ratios of 0.5 and 1.0 were investigated. All bodies tested were stable in pitch about a point one-third the body length from the nose. It was found that, in general, the basic data were linear or near linear up to an angle of attack of 8° or 10°; in some cases this linearity extended to an angle of attack of 20°.

The effect of nose corner rounding of flat-faced cylinders and spherical-faced cylinders on the aerodynamic characteristics of bodies with fineness ratios of 0.5 and 1.0 has been determined. The effects of changing the exponent of shapes generated by the power-law equation have been determined. It was found that the body having an exponent of 2 and a fineness ratio of 1.0 exhibited comparatively high lift, high stability in pitch, the lowest drag measured, and the highest ballistic coefficient measured. A comparison of the data on the exponential shapes at a Mach number of 24.5 in helium is compared with this same family of shapes at a Mach number of 3.55 in air. Higher values

of normal-force coefficient and stability in pitch obtained for the lower Mach number were attributed largely to the difference between induced pressure effects caused by the difference in Mach number and test gas. A sufficient number of shapes were tested within the corner radius and exponential investigations to permit the determination of the aerodynamic characteristics of any shape within these classes by merely fairing curves through the plotted summary data.

In general, increasing the half-angle of blunted cones from 0° to 30° improved lift and stability in pitch but decreased the ratio of internal volume to surface area. Variation of the flare half-angle of cylinder-cone frustums from 0° to 30° also produced increases in lift and stability in pitch and also decreased the ratio of internal volume to surface area.

Modified Newtonian theory generally underpredicted the normal force on bodies that had cylinders for a major portion of their geometry, but agreement between experimental and theoretical results generally improved as bluntness was decreased and, in some cases, theory overpredicted normal force on the lower drag bodies. The theory generally overpredicted axial force but agreement of theory and experiment improved as bluntness was decreased.

Langley Research Center,
National Aeronautics and Space Administration,
Langley Station, Hampton, Va., February 6, 1964.

REFERENCES

1. Chapman, Dean R.: An Approximate Analytical Method for Studying Entry Into Planetary Atmospheres. NASA TR R-11, 1959. (Supersedes NACA TN 4276.)

2. Chapman, Dean R.: An Analysis of the Corridor and Guidance Requirements for Supercircular Entry Into Planetary Atmospheres. NASA TR R-55, 1960.

3. Allen, H. Julian: Motion of a Ballistic Missile Angularly Misalined With the Flight Path Upon Entering the Atmosphere and Its Effect Upon Aerodynamic Heating, Aerodynamic Loads, and Miss Distance. NACA TN 4048, 1957. (Supersedes NACA RM A56F15.)

4. Sommer, Simon C., and Tobak, Murray: Study of the Oscillatory Motion of Manned Vehicles Entering the Earth's Atmosphere. NASA MEMO 3-2-59A, 1959.

5. Rasool, S. I.: Structure of Planetary Atmospheres. AIAA Jour., vol. 1, no. 1, Jan. 1963, pp. 6-19.

6. McDearmon, Russell W., and Lawson, Warren A.: Investigation of the Normal-Force, Axial-Force, and Pitching-Moment Characteristics of Blunt Low-Fineness-Ratio Bodies of Revolution at a Mach Number of 3.55. NASA TM X-467, 1961.

7. Johnston, Patrick J., and Snyder, Curtis D.: Static Longitudinal Stability and Performance of Several Ballistic Spacecraft Configurations in Helium at a Mach Number of 24.5. NASA TN D-1379, 1962.

8. Rainey, Robert W.: Working Charts for Rapid Prediction of Force and Pressure Coefficients on Arbitrary Bodies of Revolution by Use of Newtonian Concepts. NASA TN D-176, 1959.

9. Love, Eugene S., Henderson, Arthur, Jr., and Bertram, Mitchel H.: Some Aspects of Air-Helium Simulation and Hypersonic Approximations. NASA TN D-49, 1959.

10. Cole, J. D.: Newtonian Flow Theory for Slender Bodies. Jour. Aero. Sci., vol. 24, no. 6, June 1957, pp. 448-455.

11. Traugott, Stephen C.: Some Features of Supersonic and Hypersonic Flow About Blunted Cones. Journal Aerospace Sci., vol. 29, no. 4, Apr. 1962, pp. 389-399.

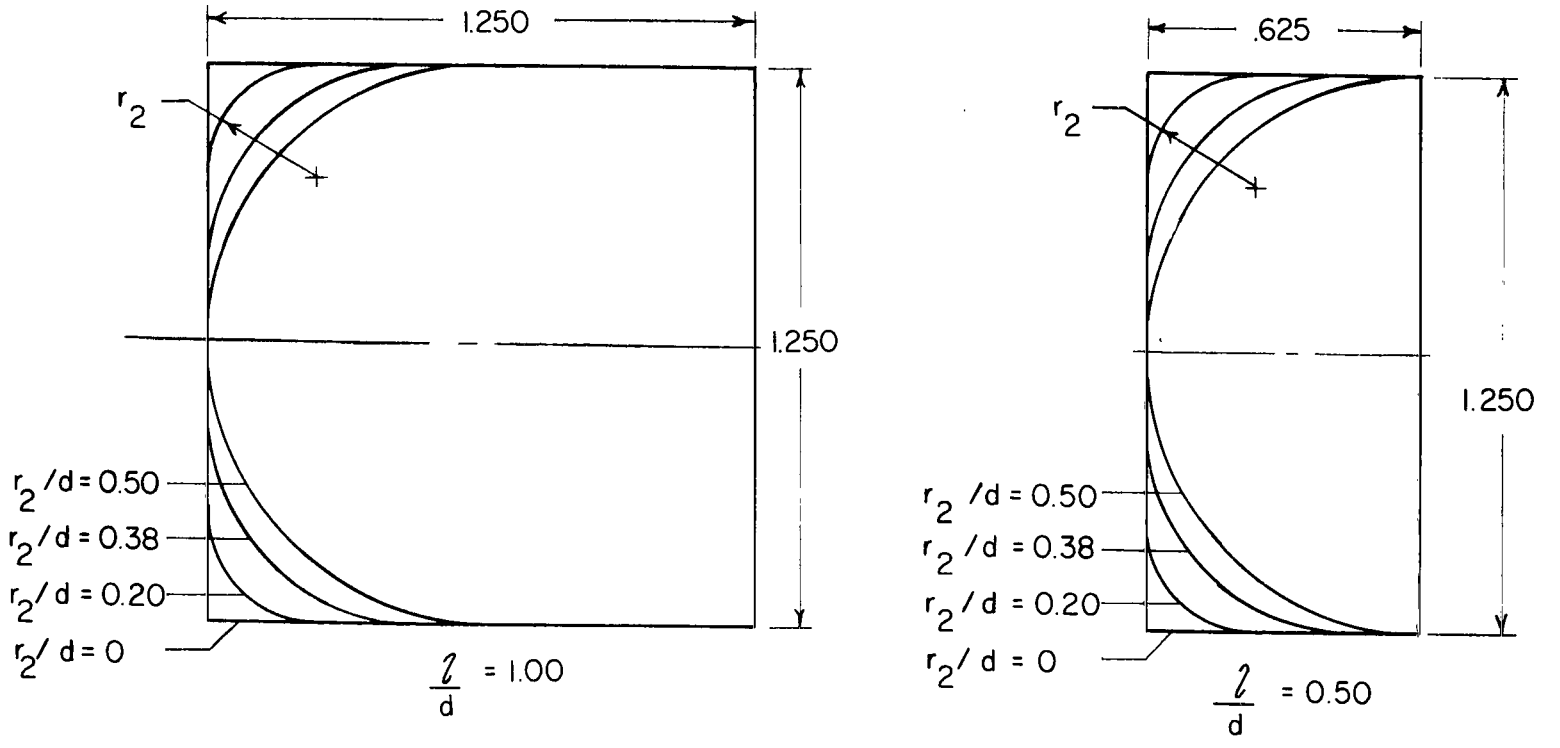

(a) Variation of corner radius of flat-faced cylinder.

Figure 1.- Drawing of models. All dimensions in inches.

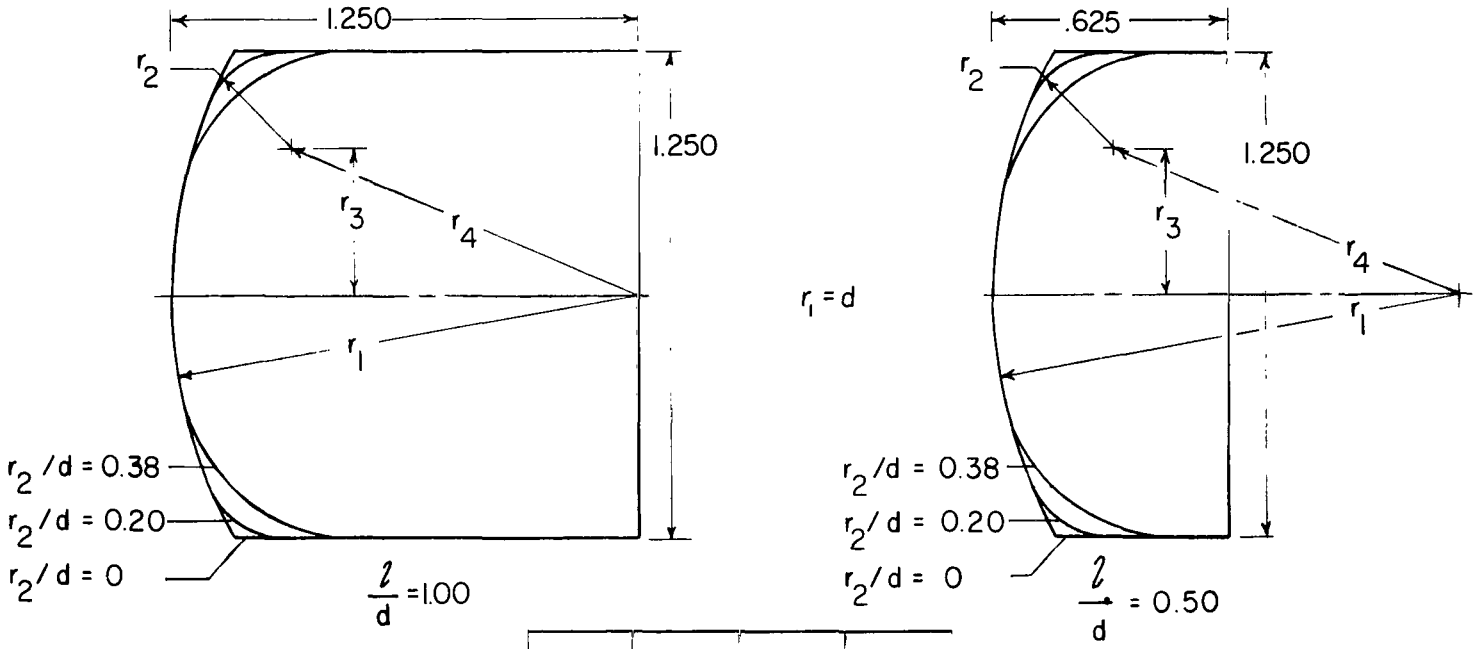

$\frac{r_2}{d}$	r_2	r_3	r_4
0	0		
0.20	.250	.375	1.000
0.38	.469	.156	.781

(b) Variation of corner radius of spherical-faced cylinders.

Figure 1.- Continued.

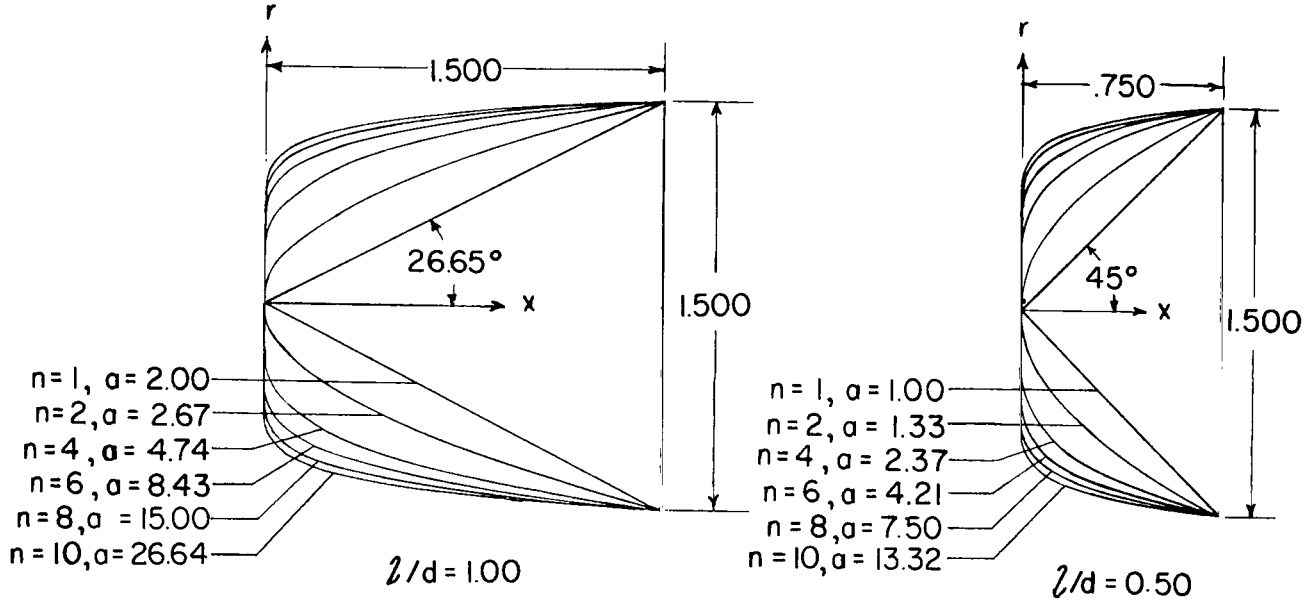

(c) Exponential shapes (shapes generated by revolving the curve generated by the equation $x = ar^n$ about the X-axis).

Figure 1.- Continued.

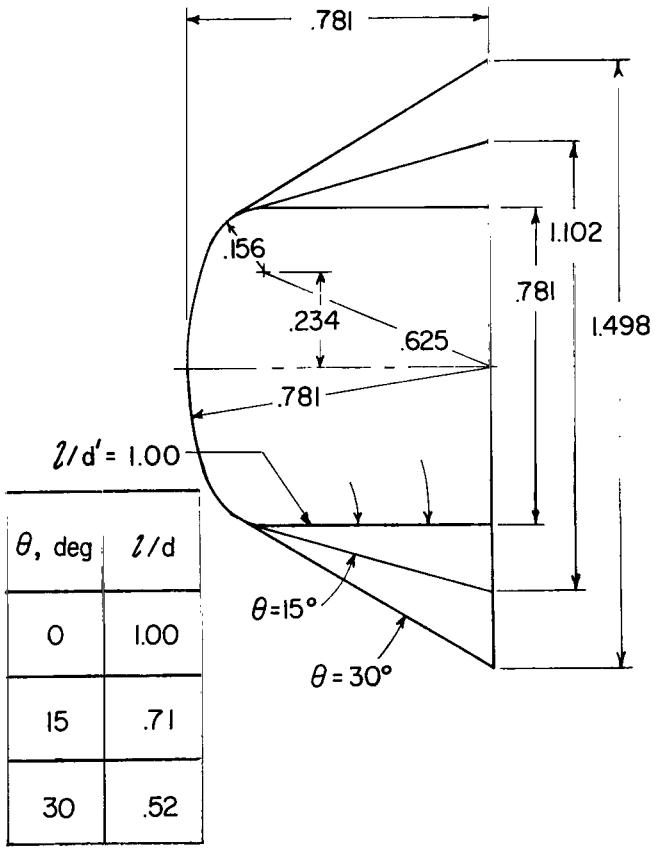

θ, deg	ℓ/d
0	1.00
15	.71
30	.52

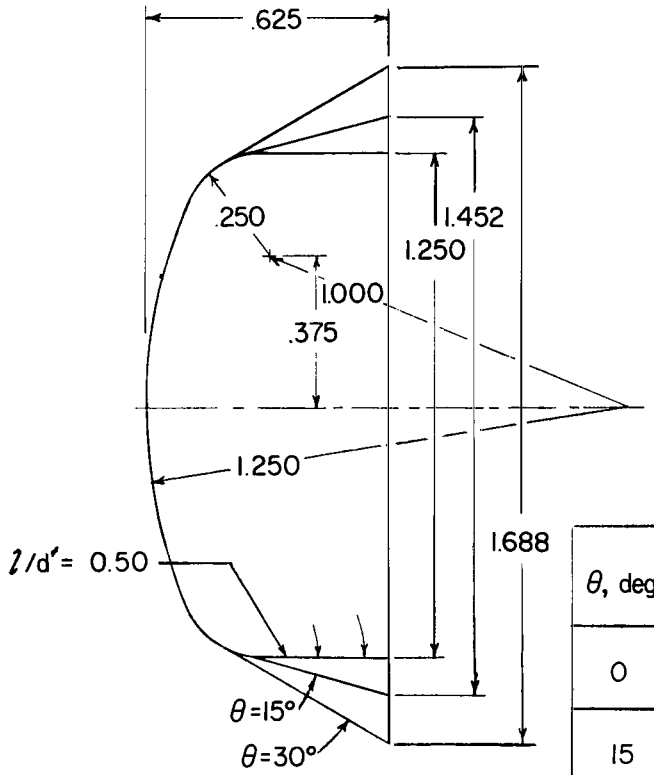

θ, deg	ℓ/d
0	.50
15	.43
30	.37

(d) Blunted cones for model with half-angle of 0°. $r_1/d = 1.00$; $r_2/d = 0.20$.

Figure 1.- Continued.

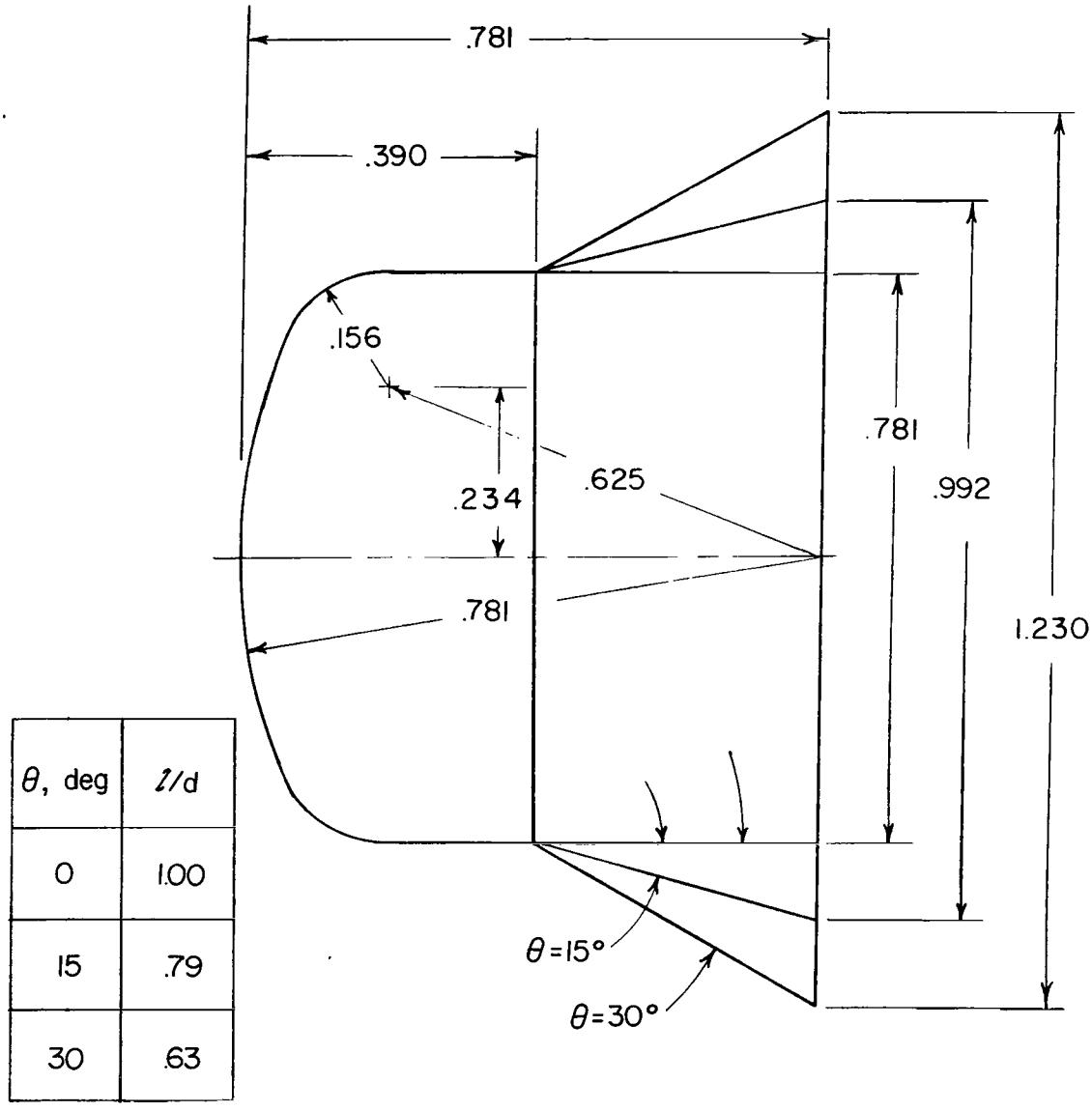

θ, deg	ℓ/d
0	1.00
15	.79
30	.63

(e) Cylinder-cone frustums for model with half-angle of 0°. $r_1/d = 1.00$; $r_2/d = 0.20$.

Figure 1.- Concluded.

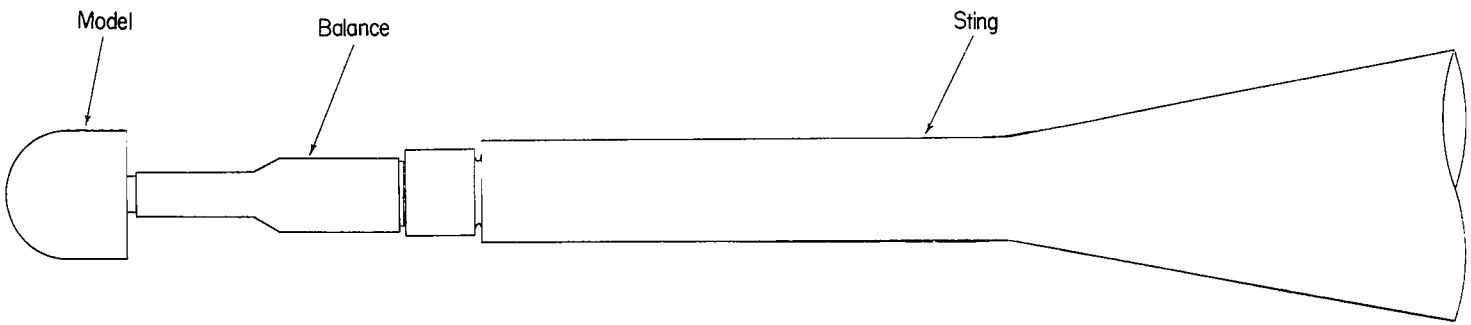

Figure 2.- Sketch of model, balance, and sting orientation.

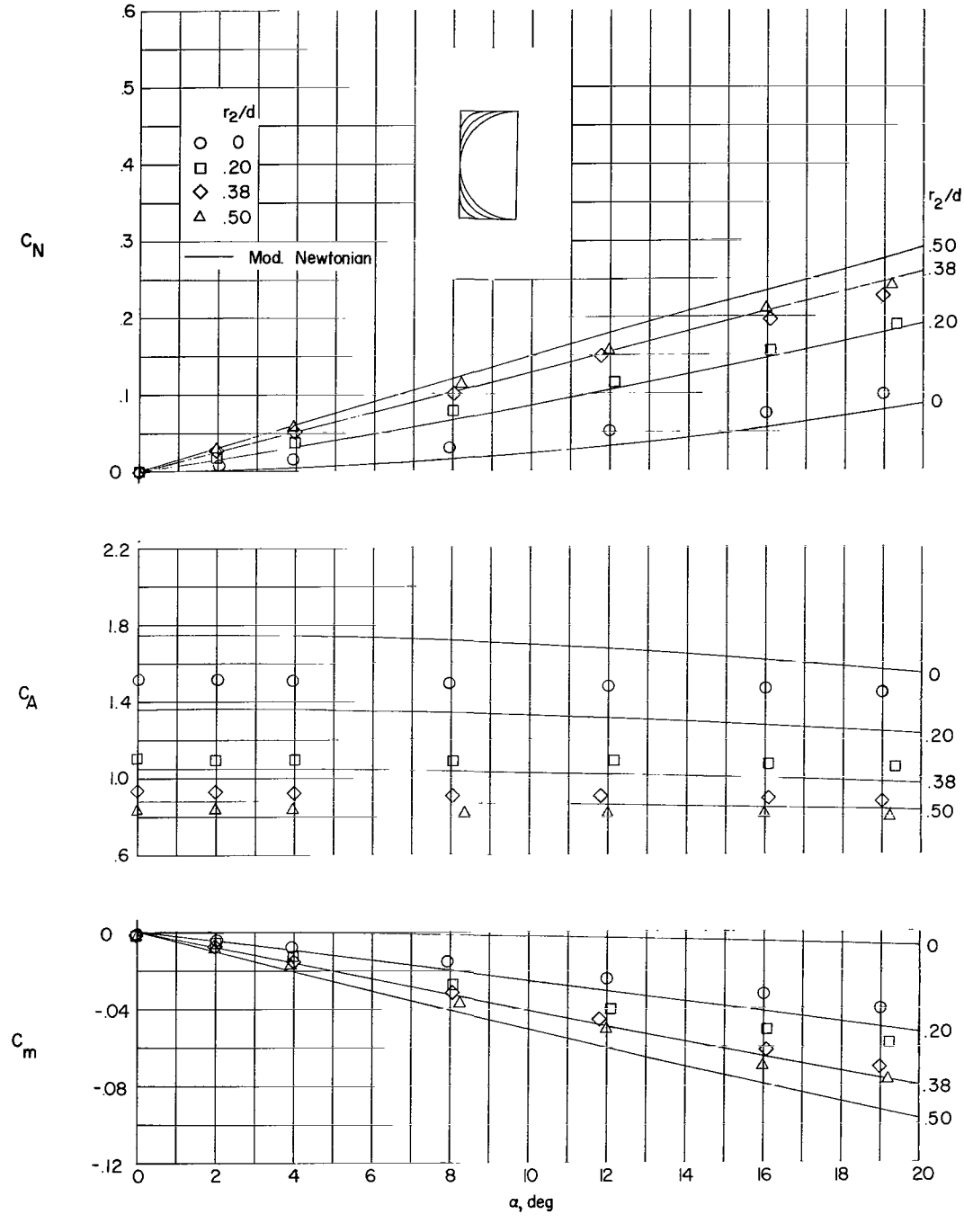

(a) Variation of C_N, C_A, and C_m with α. $l/d = 0.5$.

Figure 3.- Effect of varying corner radius on the longitudinal characteristics of a flat-faced cylinder.

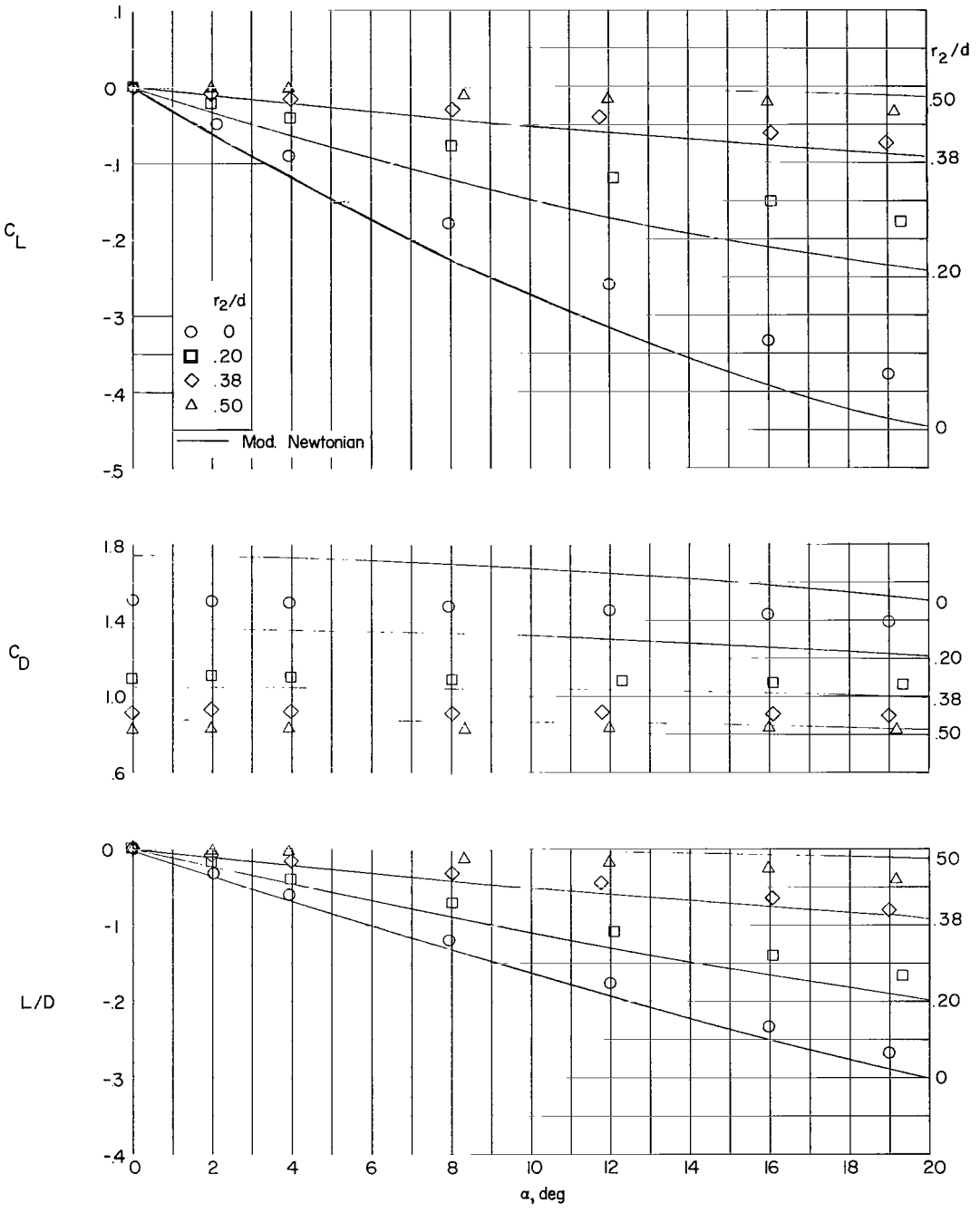

(b) Variation of C_L, C_D, and L/D with α. $l/d = 0.5$.

Figure 3.- Continued.

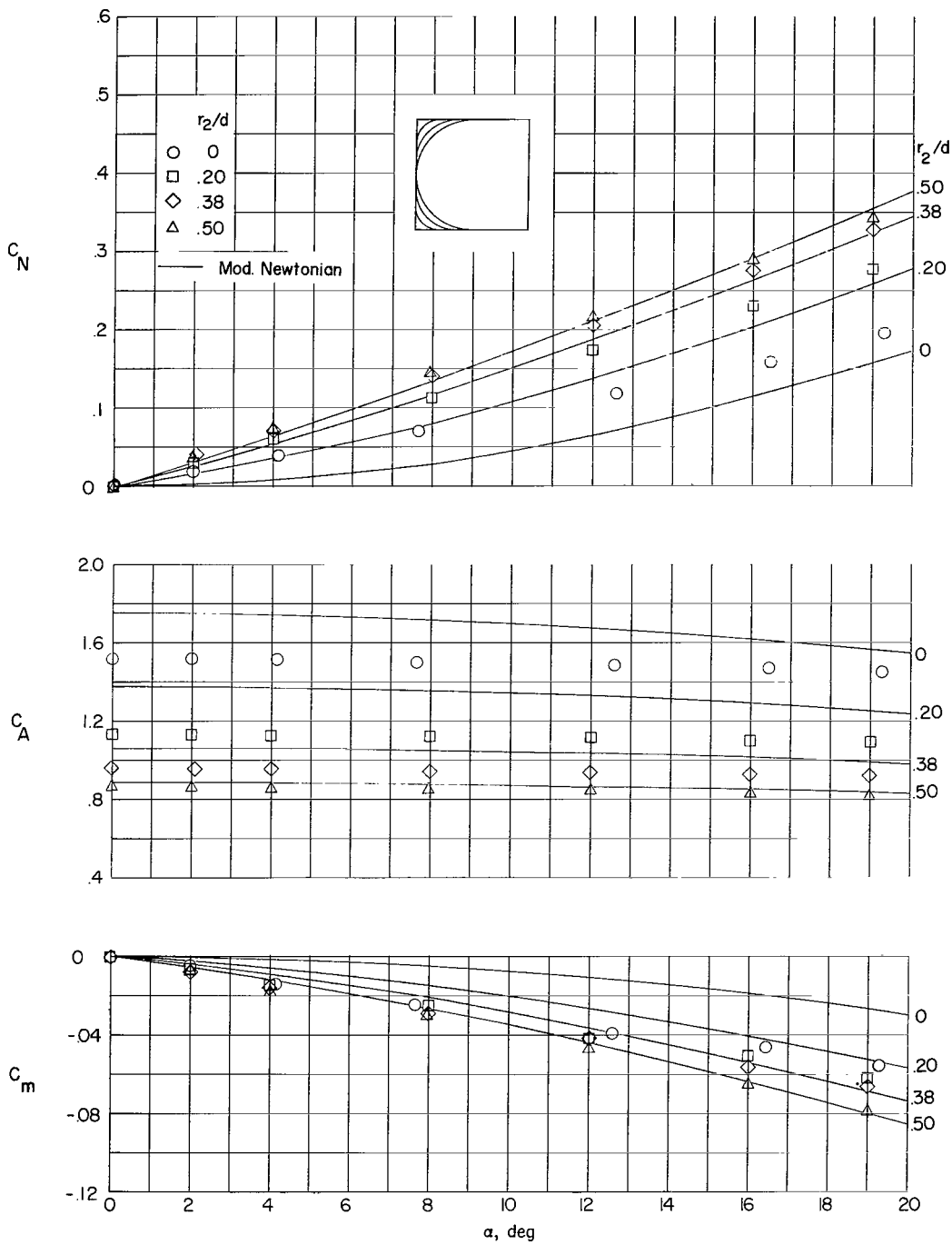

(c) Variation of C_N, C_A, and C_m with α. $l/d = 1.0$.

Figure 3.- Continued.